CHAPTER 11

Anti-amyloid drug design

Mateusz Banach[1], **Leszek Konieczny**[2], **Irena Roterman**[1]
[1]Department of Bioinformatics and Telemedicine, Jagiellonian University – Medical College, Krakow, Poland
[2]Chair of Medical Biochemistry, Jagiellonian University – Medical College, Krakow, Poland

Contents

Conceptual visualization of drug design via complexation of amphipathic helices(in red) compatible with the distribution of hydrophobicity in the fibril and exposing a hydrophilic layer, which facilitates interaction with water. This idea in based on the analysis of stop signals in proteins with linear propagation present in their structure.

If we support the conclusions which arise from applying the fuzzy oil drop model to amyloid structures and proteins which contain solenoid fragments, the process of designing drugs capable of arresting linear propagation (which leads to unrestricted growth of the molecule) should begin with the analysis of ways in which this kind of propagation is prevented in biological proteins containing amyloid-like structures.

The solenoid is a supersecondary structure which results from linear alignment of polypeptide chain fragments, much like in amyloids. Proteins in which such structures appear—mostly lyases and antifreeze proteins—provide "stop fragments" (or "caps") which prevent unrestricted propagation of solenoids. Following this observation, we performed an analysis of both groups of proteins, focusing on their caps. As it turns out, these caps may adopt various conformations—helices (in most cases), random coils and even short β-strands. Additionally, in a handful of cases, no obvious "caps" can be identified; instead the terminal fragment of the solenoid itself exhibits a distribution of hydrophobicity consistent with the micellar form.

From Globular Proteins to Amyloids
ISBN: 978-0-08-102981-7
https://doi.org/10.1016/B978-0-08-102981-7.00019-1

Such fragments can prevent further complexation without the need of a dedicated "cap".

When analyzing the role of fragments whose purpose is to prevent propagation of complexation of additional molecules (resulting in elongation of the solenoid), it is apparent that the fragment should, on the one hand, prevent access to the ordered portion of the solenoid, while on the other hand enabling contact with water and facilitating solubility.

Table 11.1 lists the structural properties of proteins where such "stopper" fragments have been found. Figs. 11.1–11.19 present hydrophobicity profiles and 3D visualizations of these structures.

Analysis of data listed in Table 11.1 indicates that the "stopper" is typically a short helix, although in some cases it may adopt the conformation of a random coil or even a short β-strand. The latter two structures must enter into a specific relation with the remainder of the solenoid (Fig. 11.1). From the point of view of drug design, the helical conformation is preferred. The "stop" fragment should meet several conditions: (1) It should exhibit affinity for the tip of the solenoid, i.e. its conformation should be compatible with that of the outermost solenoid loop (or the outermost peptide in an amyloid fibril); (2) Its outer surface should not repel water. A helix—particularly an amphipathic one—can fulfill both requirements simultaneously. In order to achieve this, the helix should be designed in such a way as to remain compatible with the distribution of hydrophobicity presented by the solenoid (or peptide which needs to be locked out), and to expose polar fragments capable of mediating contact with the aqueous environment. Examples of such short helices which meet the stated conditions and have been designed to math specific amyloid constructs are discussed in Refs. [18,19].

Designing β-strand which possess the required characteristics and are able to arrest propagation of amyloids is much harder due to requirements associated with spatial alignment with the amyloid. By its nature, a β-strand is capable of forming hydrogen bonds in two opposite directions, thus permitting complexation with other β-strands. The alignment must be such as to prevent the fold from attracting additional folds when the given fragment is bound to the solenoid. As illustrated, the orientation of such folds is tricky and complicated, and designing them poses substantial challenges. In most cases, preventing complexation of additional folds calls for another fragment, which must be oriented at an angle with respect to the surface of the amyloid (see Fig. 11.2 for an example). This unusual alignment introduces a special

Table 11.1 Values of fuzzy oil drop parameters calculated for selected structures (structural units for which the 3D Gass function was defined) and "stop" fragments found within their sequences. Asterisks (*) indicate that the β-strand treated as stop fragment is an integral part of the solenoid First line describes the protein (identified by "chain")—for this unit the 3D Gasuss function was calculated; the second line (or more) describes status of polypeptide chain fragment treated as "stopper".

Protein	Fragment		RD		Correlation coefficient			Ref.
	Structure	Residues	T-O-R	T-O-H	HvT	TvO	HvO	
2ZU0		CHAIN	0.645	0.591	0.233	0.389	0.749	[1]
	HELIX	94—104	0.259	0.372	0.446	0.818	0.745	
Antifreeze proteins								
1L0S		CHAIN	0.526	0.418	0.399	0.470	0.752	[2]
	BETA	12—15	0.217	0.140	-0.201	0.903	0.019	
	BETA	72—80	0.443	0.671	0.214	0.548	0.809	
1M8N		CHAIN	0.656	0.603	0.248	0.361	0.784	[3]
	BETA*	2—15	0.395	0.472	0.268	0.636	0.723	
	BETA*	11—15	0.312	0.161	0.353	0.873	0.356	
	RC	106—112	0.567	0.316	0.125	0.327	0.937	
3VN3		CHAIN	0.714	0.613	0.309	0.428	0.685	[4]
	BETA	48—61	0.653	0.507	-0.050	0.397	0.160	
	HELIX	100—109	0.268	0.146	0.166	0.840	0.306	
3P4G		CHAIN	0.753	0.690	0.216	0.384	0.728	[5]
	BETA	23—35	0.566	0.554	0.199	0.534	0.649	
	HELIX	285—302	0.216	0.137	0.660	0.846	0.850	
1Z2F		CHAIN	0.671	0.711	0.186	0.377	0.625	[6]
	BETA	1—7	0.497	0.682	0.295	0.431	0.898	
	RC	102—117	0.476	0.486	0.472	0.622	0.616	
1N4I		CHAIN	0.480	0.398	0.362	0.556	0.787	[7]
	RC	1—9	0.425	0.401	0.100	0.683	0.701	
	RC	71—78	0.313	0.458	0.218	0.752	0.673	
3WP9		CHAIN	0.658	0.576	0.282	0.450	0.679	[8]
	HELIX	40—54	0.671	0.640	0.243	0.069	0.618	
	MIXED	59—70	0.378	0.260	0.327	0.705	0.545	
Lyases								
1BN8		CHAIN	0.684	0.559	0.194	0.346	0.750	[9]
	HELIX	37—47	0.314	0.326	0.826	0.760	0.950	
	RC	354—364	0.416	0.396	0.100	0.657	0.469	
1PLU		CHAIN	0.654	0.540	0.234	0.388	0.749	[10]
	HELIX	26—37	0.354	0.303	0.782	0.679	0.862	
	RC	302—313	0.617	0.536	0.284	0.489	0.668	

(*Continued*)

Table 11.1 Values of fuzzy oil drop parameters calculated for selected structures (structural units for which the 3D Gass function was defined) and "stop" fragments found within their sequences. Asterisks (*) indicate that the β-strand treated as stop fragment is an integral part of the solenoid First line describes the protein (identified by "chain")—for this unit the 3D Gasuss function was calculated; the second line (or more) describes status of polypeptide chain fragment treated as "stopper".—cont'd

Protein	Fragment		RD		Correlation coefficient			Ref.
	Structure	Residues	T-O-R	T-O-H	HvT	TvO	HvO	
2FKO		CHAIN	0.457	0.405	0.332	0.584	0.744	[11]
	BETA	1–6	0.207	0.257	0.487	0.896	0.633	
	BETA	137–144	0.400	0.163	0.531	0.652	0.794	
1QRM		CHAIN	0.475	0.471	0.363	0.661	0.737	[12]
	RC	5–9	0.591	0.214	0.164	0.961	0.311	
	HELIX	176–183	0.373	0.223	0.523	0.685	0.846	
1QRG		CHAIN	0.418	0.418	0.400	0.716	0.745	[12]
	RC	8–14	0.750	0.146	-0.317	0.712	0.138	
	HELIX	176–183	0.294	0.146	0.567	0.817	0.873	
1IDJ		CHAIN	0.722	0.650	0.216	0.313	0.737	[13]
	HELIX	27–36	0.255	0.258	0.727	0.868	0.937	
1OOC		CHAIN	0.643	0.501	0.238	0.429	0.704	[14]
	HELIX	39–50	0.369	0.296	0.809	0.716	0.829	
	RC	318–328	0.434	0.761	0.689	0.528	0.930	
1O88		CHAIN	0.650	0.541	0.230	0.392	0.748	[15]
	HELIX	25–37	0.382	0.325	0.781	0.644	0.856	
	RC	308–312	0.655	0.567	0.976	0.415	0.507	
1JRG		CHAIN	0.649	0.487	0.241	0.420	0.701	[16]
	HELIX	41–50	0.376	0.322	0.824	0.711	0.844	
	RC	320–327	0.457	0.848	0.574	0.459	0.970	
1JTA		CHAIN	0.632	0.489	0.240	0.440	0.706	[16]
	HELIX	40–51	0.402	0.344	0.832	0.650	0.811	
	RC	318–329	0.382	0.749	0.725	0.626	0.934	
2BSP		CHAIN	0.688	0.558	0.187	0.332	0.750	[17]
	HELIX	37–46	0.304	0.615	0.783	0.740	0.932	
	RC	349–364	0.450	0.463	0.241	0.637	0.625	

requirement, which is difficult to satisfy when designing β "stoppers". In addition, a putative short β-strand capable of arresting amyloid growth, may fail to retain its structural characteristics when isolated.

For the reasons stated above we believe that only a helical fragment, which is highly stable on its own, may serve as an efficient "stopper"—as long as it remains compatible with the target amyloid.

The relationship between "stop" fragments and the entirety of the molecule becomes even more transparent in the context of solenoids equipped

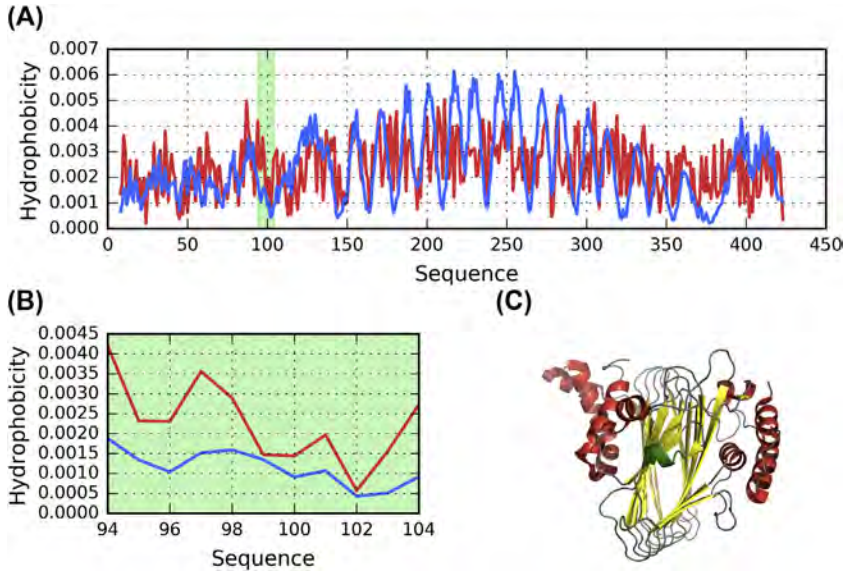

Fig. 11.1 FOD characteristic of sufc-sufd complex involved in the iron-sulfur cluster biosynthesis (2ZU0): (A)—hydrophobicity distribution profiles: T (blue), O (red); green background—"stopper(s)". (B)—detailed view of profiles from A, focused on "stop" fragment(s) only. (C)—3D presentation of the protein (green color—"stopper(s)", N-terminal in the foreground).

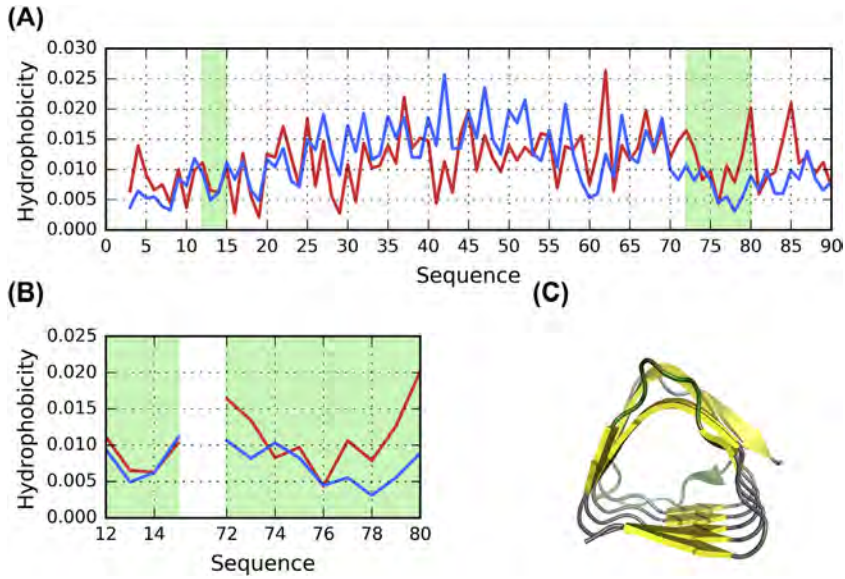

Fig. 11.2 FOD characteristic of antifreeze protein from *Choristoneura fumiferana* (1L0S): (A) hydrophobicity distribution profiles: T (blue), O (red); green background—" stopper(s)". (B) detailed view of profiles from A, focused on "stop" fragment(s) only. (C) 3D presentation of the protein (green color—"stopper(s)", N-terminal in the foreground).

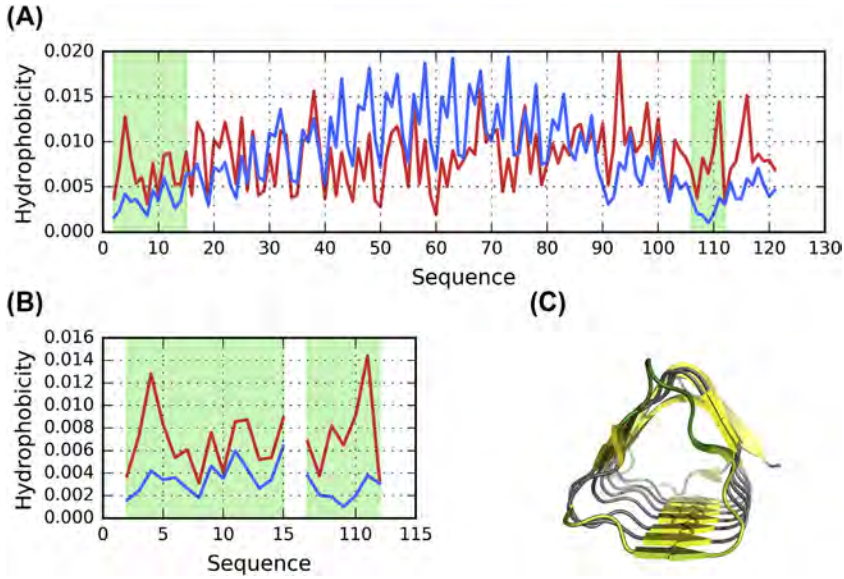

Fig. 11.3 FOD characteristic of antifreeze protein from *Choristoneura fumiferana* (1M8N): (A) hydrophobicity distribution profiles: T (blue), O (red); green background—" stopper(s)". (B) detailed view of profiles from A, focused on "stop" fragment(s) only. (C) 3D presentation of the protein (green color—"stopper(s)", N-terminal in the foreground).

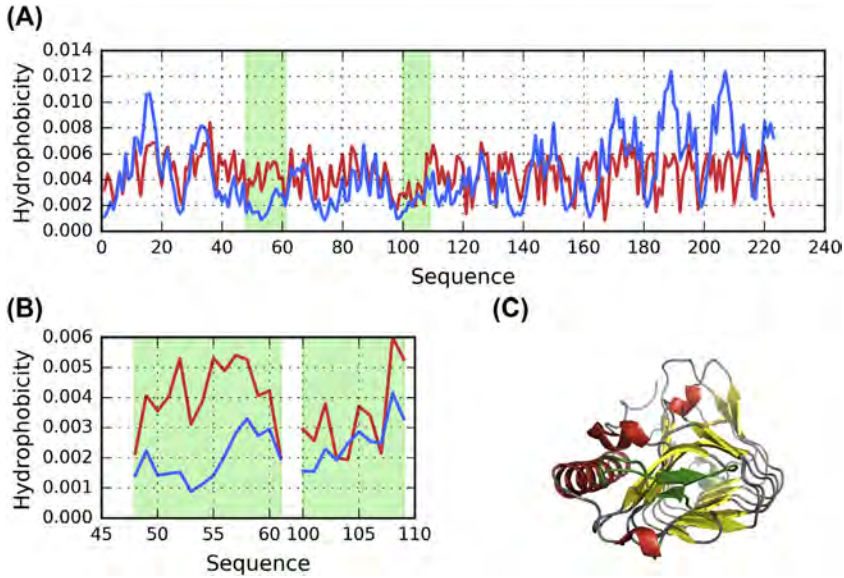

Fig. 11.4 FOD characteristic of fungal antifreeze protein from Typhula ishikariensis. (3VN3): (A) hydrophobicity distribution profiles: T (blue), O (red); green background—" stopper(s)". (B) detailed view of profiles from A, focused on "stop" fragment(s) only. (C) 3D presentation of the protein (green color—"stopper(s)", N-terminal in the foreground).

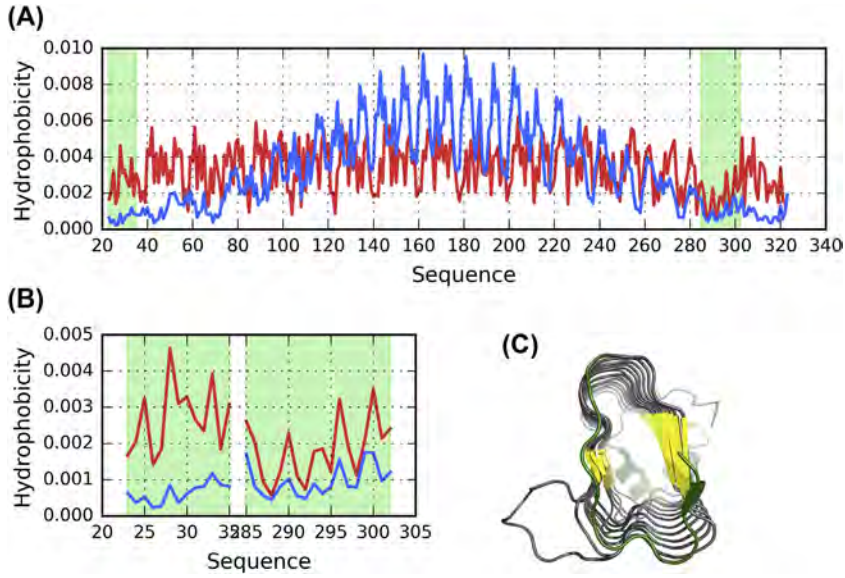

Fig. 11.5 FOD characteristic of bacterial antifreeze protein from *Marinomonas primoryensis* (3P4G): (A) hydrophobicity distribution profiles: T (blue), O (red); green background—"stopper(s)". (B) detailed view of profiles from A, focused on "stop" fragment(s) only. (C) 3D presentation of the protein (green color—"stopper(s)", N-terminal in the foreground).

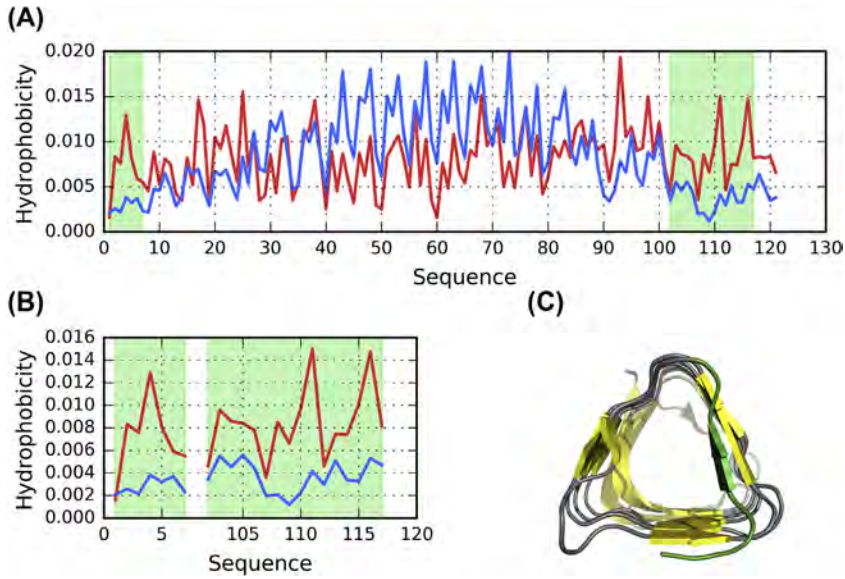

Fig. 11.6 FOD characteristic of antifreeze protein from spruce budworm (*Choristoneura fumiferana*.) (1Z2F): (A) hydrophobicity distribution profiles: T (blue), O (red); green background—"stopper(s)". (B) detailed view of profiles from A, focused on "stop" fragment(s) only. (C) 3D presentation of the protein (green color—"stopper(s)", N-terminal in the foreground).

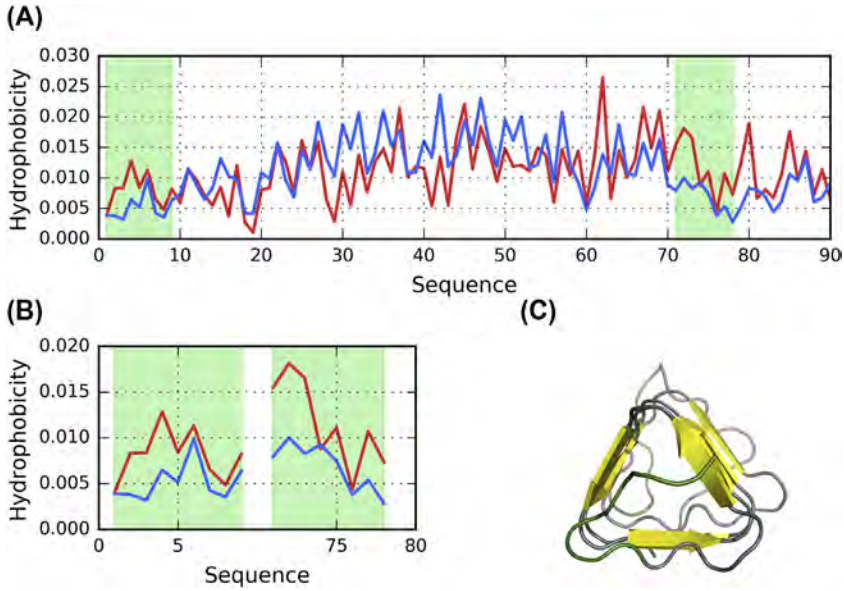

Fig. 11.7 FOD characteristic of antifreeze protein from Spruce budworm. (*Choristoneura fumiferana*). (1N4I): (A) hydrophobicity distribution profiles: T (blue), O (red); green background—"stopper(s)". (B) detailed view of profiles from A, focused on "stop" fragment(s) only. (C) 3D presentation of the protein (green color—"stopper(s)", N-terminal in the foreground).

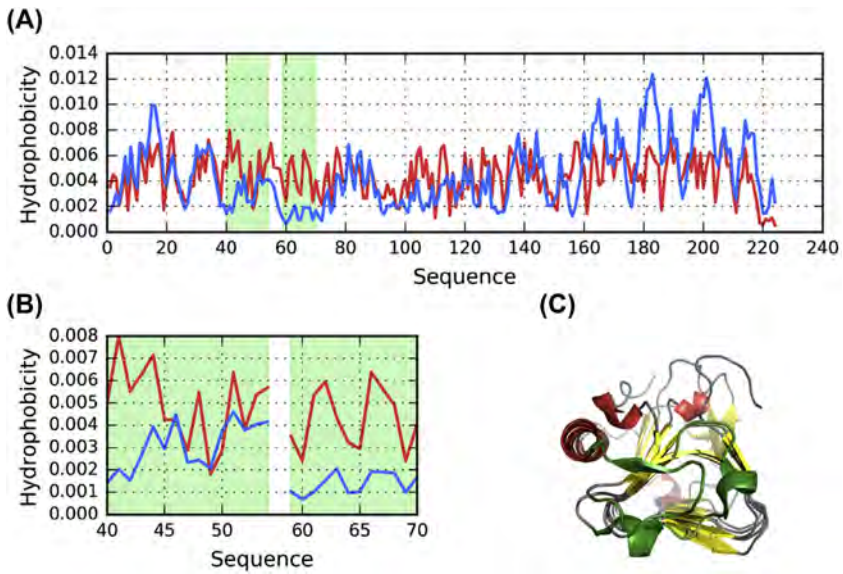

Fig. 11.8 FOD characteristic of antifreeze protein from an antarctic sea ice bacterium *colwellia sp* (3WP9): (A) hydrophobicity distribution profiles: T (blue), O (red); green background—"stopper(s)". (B) detailed view of profiles from A, focused on "stop" fragment(s) only. (C) 3D presentation of the protein (green color—"stopper(s)", N-terminal in the foreground).

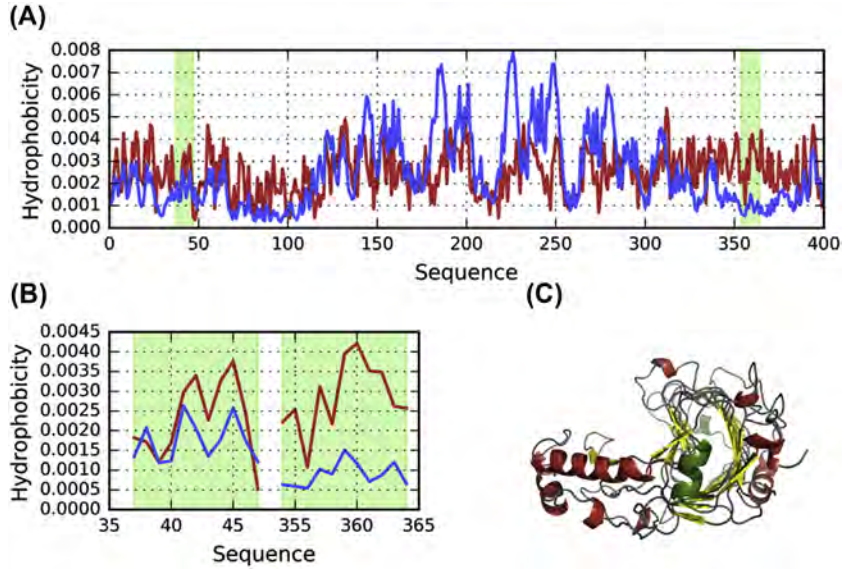

Fig. 11.9 FOD characteristic of Bacillus subtilis pectate lyase (1BN8): (A) hydrophobicity distribution profiles: T (blue), O (red); green background—"stopper(s)". (B) detailed view of profiles from A, focused on "stop" fragment(s) only. (C) 3D presentation of the protein (green color—"stopper(s)", N-terminal in the foreground).

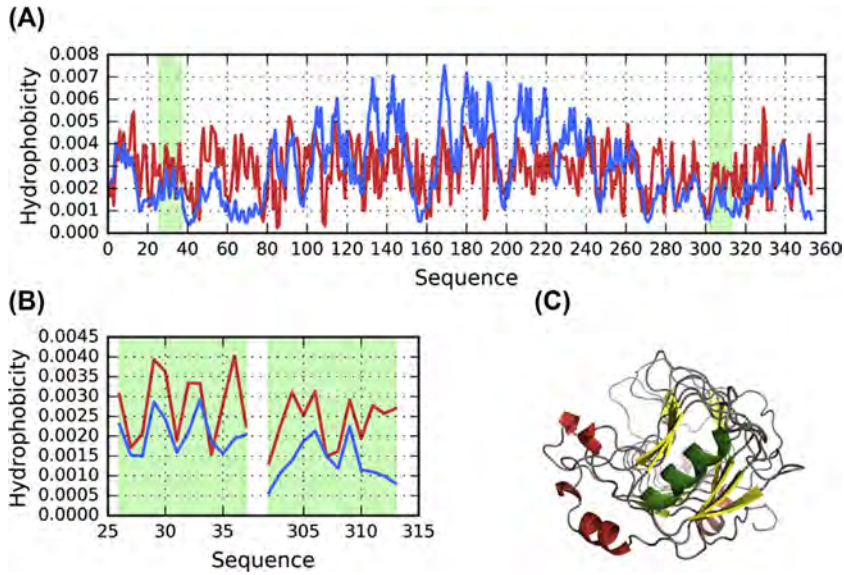

Fig. 11.10 FOD characteristic of pectate lyase C from erwinia chrysanthemi with 1 lu+3 ion in the putative calcium binding site (1PLU): (A) hydrophobicity distribution profiles: T (blue), O (red); green background—"stopper(s)". (B) detailed view of profiles from A, focused on "stop" fragment(s) only. (C) 3D presentation of the protein (green color—" stopper(s)", N-terminal in the foreground).

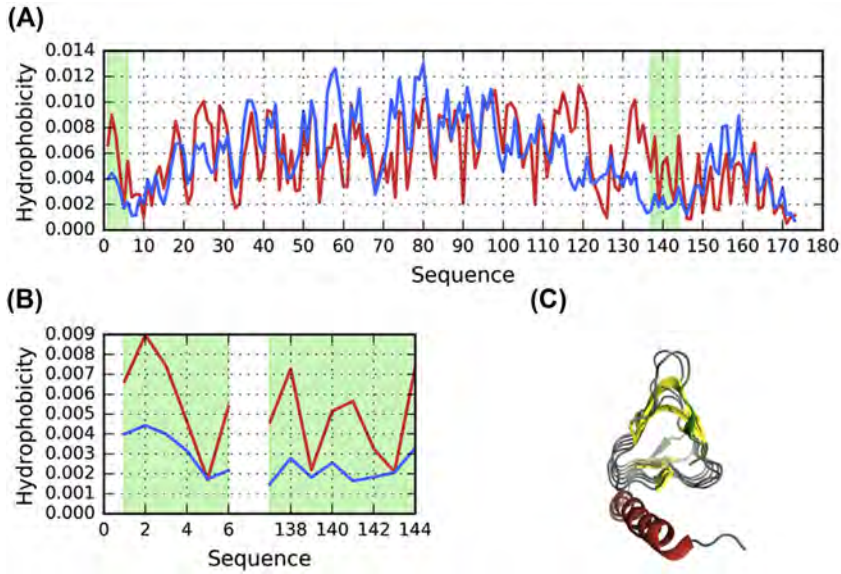

Fig. 11.11 FOD characteristic of carbonic anhydrase from *Pyrococcus horikoshii.* (2FKO): (A) hydrophobicity distribution profiles: T (blue), O (red); green background—" stopper(s)". (B) detailed view of profiles from A, focused on "stop" fragment(s) only. (C) 3D presentation of the protein (green color—"stopper(s)", N-terminal in the foreground).

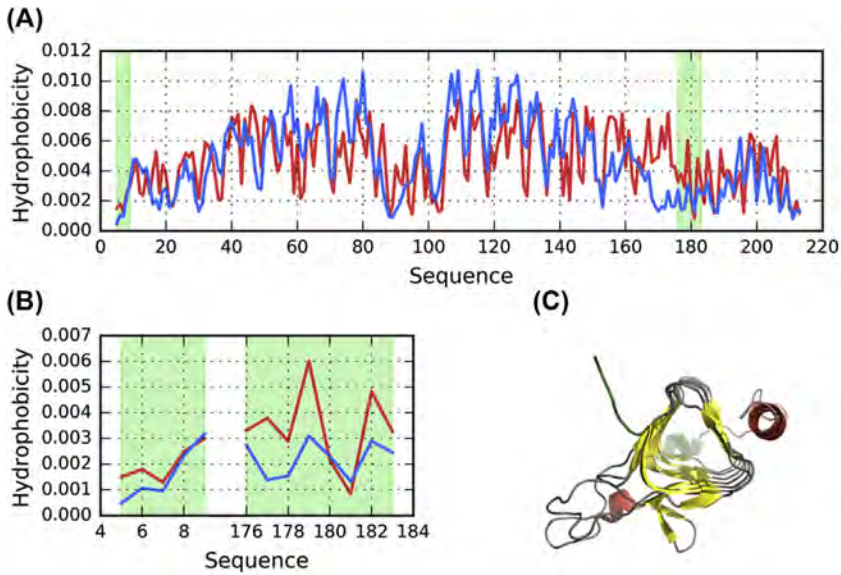

Fig. 11.12 FOD characteristic of carbonic anhydrase from *Methanosarcina thermophila* (1QRM): (A) hydrophobicity distribution profiles: T (blue), O (red); green background—" stopper(s)". (B) detailed view of profiles from A, focused on "stop" fragment(s) only. (C) 3D presentation of the protein (green color—"stopper(s)", N-terminal in the foreground).

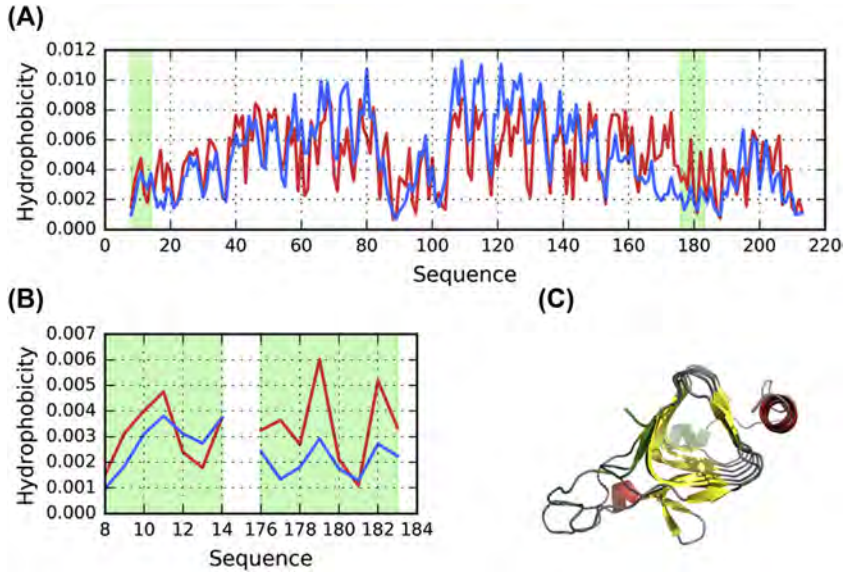

Fig. 11.13 FOD characteristic of carbonic anhydrase from *methanosarcina thermophila* (1QRG): (A) hydrophobicity distribution profiles: T (blue), O (red); green background—" stopper(s)". (B) detailed view of profiles from A, focused on "stop" fragment(s) only. (C) 3D presentation of the protein (green color—"stopper(s)", N-terminal in the foreground).

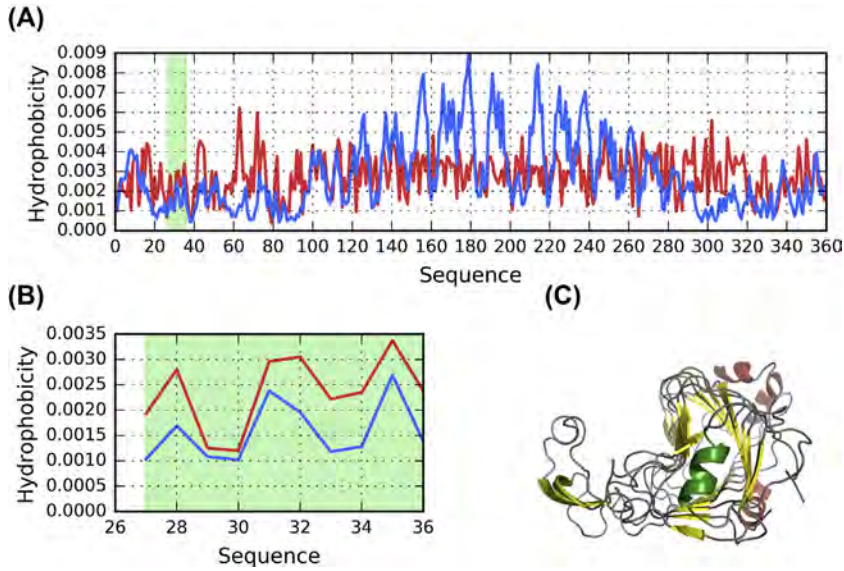

Fig. 11.14 FOD characteristic of pectin lyase from *Aspergillus niger*. (1IDJ): (A) hydrophobicity distribution profiles: T (blue), O (red); green background—" stopper(s)". (B) detailed view of profiles from A, focused on "stop" fragment(s) only. (C) 3D presentation of the protein (green color—"stopper(s)", N-terminal in the foreground).

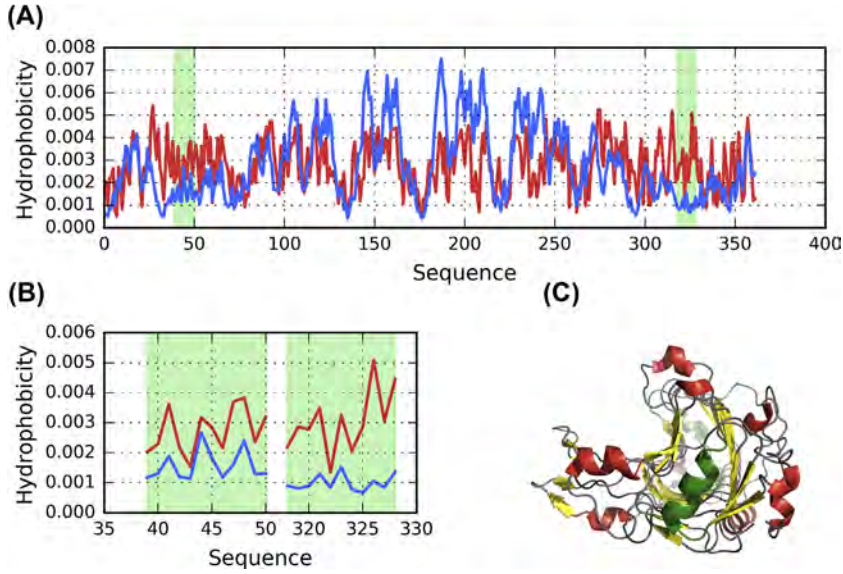

Fig. 11.15 FOD characteristic of pectate lyase from *Erwinia chrysanthem* (1OOC): (A) hydrophobicity distribution profiles: T (blue), O (red); green background—" stopper(s)". (B) detailed view of profiles from A, focused on "stop" fragment(s) only. (C) 3D presentation of the protein (green color—"stopper(s)", N-terminal in the foreground).

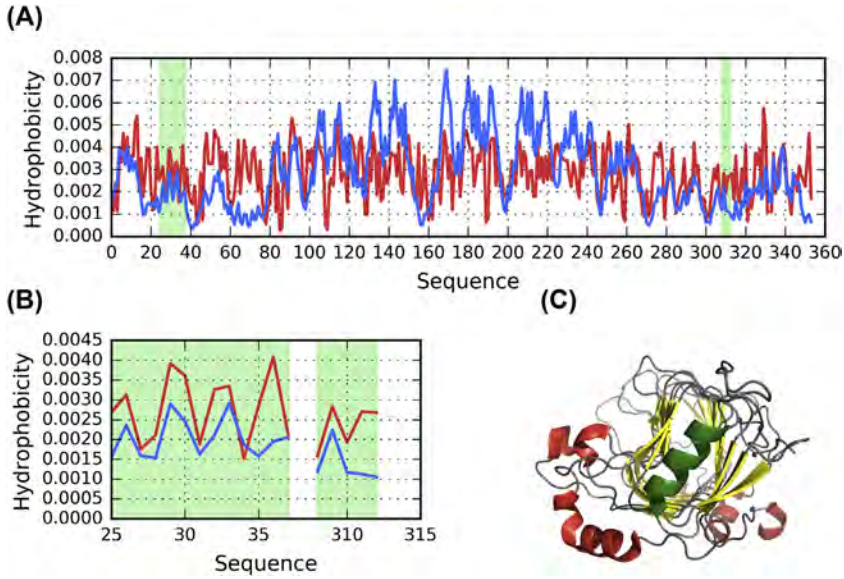

Fig. 11.16 FOD characteristic of pectate lyase C from *Erwinia chrysanthemi* (1O88): (A) hydrophobicity distribution profiles: T (blue), O (red); green background—" stopper(s)". (B) detailed view of profiles from A, focused on "stop" fragment(s) only. (C) 3D presentation of the protein (green color—"stopper(s)", N-terminal in the foreground).

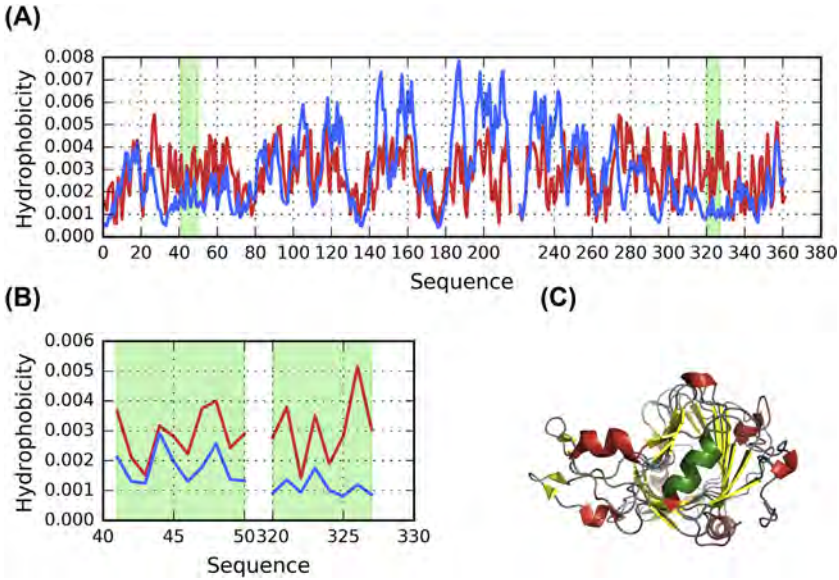

Fig. 11.17 FOD characteristic of pectate lyase from *Erwinia chrysanthemi* (1JRG): (A) hydrophobicity distribution profiles: T (blue), O (red); green background—" stopper(s)". (B) detailed view of profiles from A, focused on "stop" fragment(s) only. (C) 3D presentation of the protein (green color—"stopper(s)", N-terminal in the foreground).

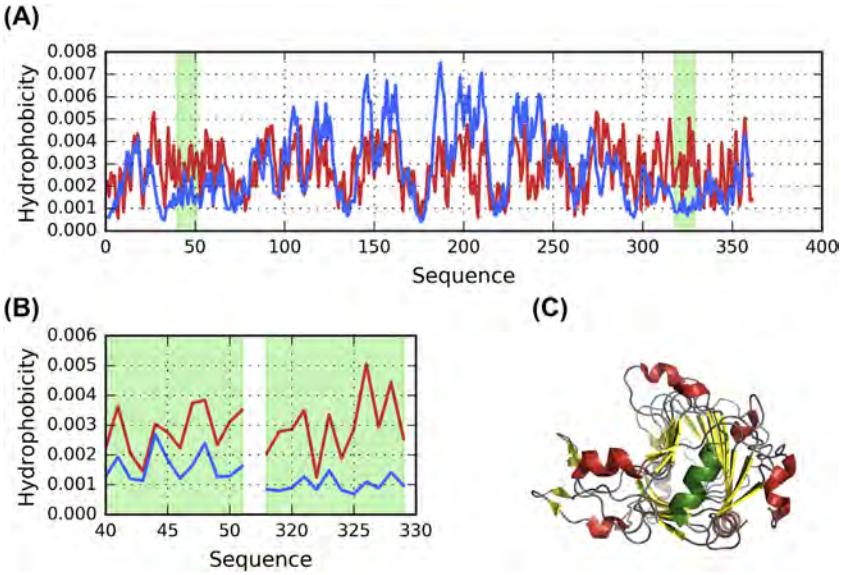

Fig. 11.18 FOD characteristic of pectate lyase from *Erwinia chrysanthemi*. (1JTA): (A) hydrophobicity distribution profiles: T (blue), O (red); green background—" stopper(s)". (B) detailed view of profiles from A, focused on "stop" fragment(s) only. (C) 3D presentation of the protein (green color—"stopper(s)", N-terminal in the foreground).

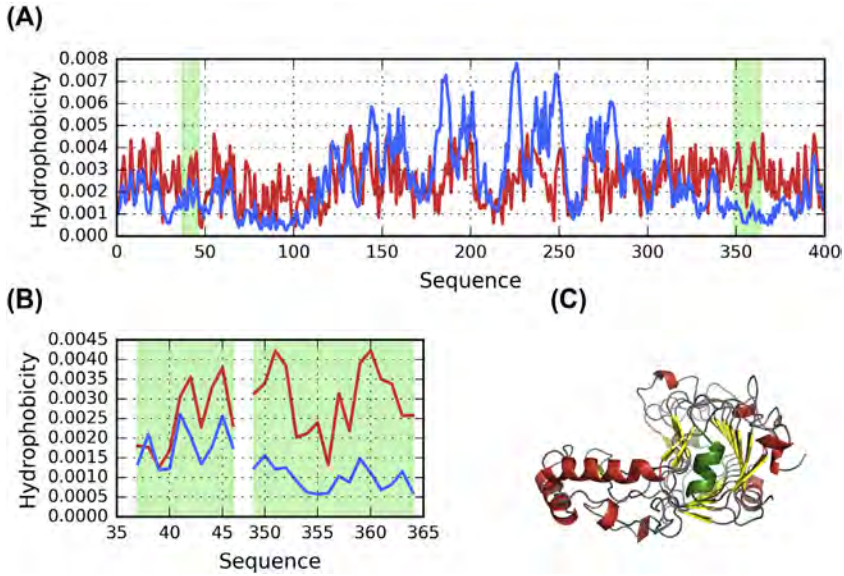

Fig. 11.19 FOD characteristic of pectate lyase from *Bacillus subtilis* (2BSP): (A) hydrophobicity distribution profiles: T (blue), O (red); green background—"stopper(s)". (B) detailed view of profiles from A, focused on "stop" fragment(s) only. (C) 3D presentation of the protein (green color—"stopper(s)", N-terminal in the foreground).

with such "stoppers". We discuss the structural properties of solenoid fragments in a separate chapter (see Chapter 7).

When discussing potential drugs capable of counteracting linear propagation of polypeptide chains (including amyloids), we should not neglect to acknowledge other proposals [20–40]. While the presented work focuses on peptide "stoppers", much research has been directed toward investigating organic compounds capable of meeting this goal [20–40]. Where peptides are mentioned, the authors usually focus their attention at β-strand—however, as noted above, designing such stoppers appears far more challenging than coming up with their helical equivalents. It is also worth noting—when looking at the contents of Table 11.1—that in all biological proteins the role of "caps" falls to helical fragments.

References

[1] Wada K, Sumi N, Nagai R, Iwasaki K, Sato T, Suzuki K, Fukuyama K. Molecular dynamism of Fe–S cluster biosynthesis implicated by the structure of the SufC2–SufD2 complex. Journal of Molecular Biology 2009;387(1):245–58. https://doi.org/10.1016/j.jmb.2009.01.054.

[2] Leinala EK, Davies PL, Jia Z. Crystal structure of β-helical antifreeze protein points to a general ice binding model. Structure 2002;10(5):619–27. https://doi.org/10.1016/s0969-2126(02)00745-1.
[3] Leinala EK. A beta -helical antifreeze protein isoform with increased activity. Structural and functional insights. Journal of Biological Chemistry 2002;277(36):33349–52. https://doi.org/10.1074/jbc.m205575200.
[4] Kondo H, Hanada Y, Sugimoto H, Hoshino T, Garnham CP, Davies PL, Tsuda S. Ice-binding site of snow mold fungus antifreeze protein deviates from structural regularity and high conservation. Proceedings of the National Academy of Sciences 2012; 109(24):9360–5. https://doi.org/10.1073/pnas.1121607109.
[5] Garnham CP, Campbell RL, Davies PL. Anchored clathrate waters bind antifreeze proteins to ice. Proceedings of the National Academy of Sciences 2011;108(18): 7363–7. https://doi.org/10.1073/pnas.1100429108.
[6] Li C, Guo X, Jia Z, Xia B, Jin C. Solution structure of an antifreeze protein CfAFP-501 from Choristoneura fumiferana. Journal of Biomolecular NMR 2005;32(3): 251–6. https://doi.org/10.1007/s10858-005-8206-3.
[7] Graether SP, Gagné SM, Spyracopoulos L, Jia Z, Davies PL, Sykes BD. Spruce budworm antifreeze protein: changes in structure and dynamics at low temperature. Journal of Molecular Biology 2003;327(5):1155–68. https://doi.org/10.1016/s0022-2836(03)00235-3.
[8] Hanada Y, Nishimiya Y, Miura A, Tsuda S, Kondo H. Hyperactive antifreeze protein from an Antarctic sea ice bacterium Colwelliasp has a compound ice-binding site without repetitive sequences. FEBS Journal 2014;281(16):3576–90. https://doi.org/10.1111/febs.12878.
[9] Pickersgill R, Jenkins J, Harris G, Nasser W, Robert-Baudouy J. The structure of Bacillus subtilis pectate lyase in complex with calcium. Nature Structural & Molecular Biology 1994;1(10):717–23. https://doi.org/10.1038/nsb1094-717.
[10] Yoder MD, Jurnak F. The refined three-dimensional structure of pectate lyase C from erwinia chrysanthemi at 2.2 Angstrom resolution (implications for an enzymatic mechanism). Plant Physiology 1995;107(2):349–64. https://doi.org/10.1104/pp.107.2.349.
[11] Jeyakanthan J, Rangarajan S, Mridula P, Kanaujia SP, Shiro Y, Kuramitsu S, Sekar K. Observation of a calcium-binding site in the γ-class carbonic anhydrase from Pyrococcus horikoshii. Acta Crystallographica Section D Biological Crystallography 2008; 64(10):1012–9. https://doi.org/10.1107/s0907444908024323.
[12] Iverson TM, Alber BE, Kisker C, Ferry JG, Rees DC. A closer look at the active site of γ-class carbonic anhydrases: high-resolution crystallographic studies of the carbonic anhydrase from Methanosarcina thermophila. Biochemistry 2000;39(31):9222–31. https://doi.org/10.1021/bi000204s.
[13] Mayans O, Scott M, Connerton I, Gravesen T, Benen J, Visser J, Jenkins J. Two crystal structures of pectin lyase A from Aspergillus reveal a pH driven conformational change and striking divergence in the substrate-binding clefts of pectin and pectate lyases. Structure 1997;5(5):677–89. https://doi.org/10.1016/s0969-2126(97)00222-0.
[14] Dehdashti SJ, Doan CN, Chao KL, Yoder MD. Effect of mutations in the T1.5 loop of pectate lyase A from Erwinia chrysanthemi EC16. Acta Crystallographica Section D Biological Crystallography 2003;59(7):1339–42. https://doi.org/10.1107/s0907444903011491.
[15] Herron SR, Scavetta RD, Garrett M, Legner M, Jurnak F. Characterization and implications of Ca^{2+} Binding to pectate lyase C. Journal of Biological Chemistry 2003; 278(14):12271–7. https://doi.org/10.1074/jbc.m209306200.

[16] Thomas LM, Doan CN, Oliver RL, Yoder MD. Structure of pectate lyase A: comparison to other isoforms. Acta Crystallographica Section D Biological Crystallography 2002;58(6):1008–15. https://doi.org/10.1107/s0907444902005851.
[17] Pickersgill, R. Bacillus subtilis pectate lyase r279k mutant. https://www.rcsb.org/structure/2BSP.
[18] Roterman I, Banach M, Konieczny L. Propagation of fibrillar structural forms in proteins stopped by naturally occurring short polypeptide chain fragments. Pharmaceuticals 2017;10(4):E89. https://doi.org/10.3390/ph10040089. pii.
[19] Roterman I, Banach M, Konieczny L. Towards the design of anti-amyloid short peptide helices. Bioinformation 2018;14(1):1–7. https://doi.org/10.6026/97320630014001. eCollection 2018.
[20] Baggett DW, Nath A. The rational discovery of a tau aggregation inhibitor. Biochemistry 2018;57(42):6099–107. https://doi.org/10.1021/acs.biochem.8b00581.
[21] Becker M, Moore A, Naughton M, Boland B, Siems W-E, Walther T. Neprilysin degrades murine Amyloid-β (Aβ) more efficiently than human Aβ: further implication for species-specific amyloid accumulation. Neuroscience Letters 2018;686:74–9. https://doi.org/10.1016/j.neulet.2018.08.028.
[22] Brumshtein B, Esswein SR, Salwinski L, Phillips ML, Ly AT, Cascio D, Eisenberg DS. Inhibition by small-molecule ligands of formation of amyloid fibrils of an immunoglobulin light chain variable domain. eLife 2015;4. https://doi.org/10.7554/elife.10935.
[23] Cao Q, Shin WS, Chan H, Vuong CK, Dubois B, Li B, Jiang L. Inhibiting amyloid-β cytotoxicity through its interaction with the cell surface receptor LilrB2 by structure-based design. Nature Chemistry 2018;10(12):1213–21. https://doi.org/10.1038/s41557-018-0147-z.
[24] Cox D, Whiten DR, Brown JWP, Horrocks MH, San Gil R, Dobson CM, Ecroyd H. The small heat shock protein Hsp27 binds α-synuclein fibrils, preventing elongation and cytotoxicity. Journal of Biological Chemistry 2018;293(12):4486–97. https://doi.org/10.1074/jbc.m117.813865.
[25] Cremades N, Dobson CM. The contribution of biophysical and structural studies of protein self-assembly to the design of therapeutic strategies for amyloid diseases. Neurobiology of Disease 2018;109:178–90. https://doi.org/10.1016/j.nbd.2017.07.009.
[26] Davis IW, Raha K, Head MS, Baker D. Blind docking of pharmaceutically relevant compounds using RosettaLigand. Protein Science 2009;18(9):1998–2002. https://doi.org/10.1002/pro.192.
[27] Filippi L, Chiaravalloti A, Bagni O, Schillaci O. ^{18}F-labeled radiopharmaceuticals for the molecular neuroimaging of amyloid plaques in Alzheimer's disease. American Journal of Nuclear Medicine and Molecular Imaging 2018;8(4):268–81.
[28] Giorgetti S, Greco C, Tortora P, Aprile F. Targeting amyloid aggregation: an overview of strategies and mechanisms. International Journal of Molecular Sciences 2018;19(9):2677. https://doi.org/10.3390/ijms19092677.
[29] Gorantla NV, Chinnathambi S. Tau protein squired by molecular chaperones during alzheimer's disease. Journal of Molecular Neuroscience 2018;66(3):356–68. https://doi.org/10.1007/s12031-018-1174-3.
[30] Kundel F, De S, Flagmeier P, Horrocks MH, Kjaergaard M, Shammas SL, Klenerman D. Hsp70 inhibits the nucleation and elongation of tau and sequesters tau aggregates with high affinity. ACS Chemical Biology 2018;13(3):636–46. https://doi.org/10.1021/acschembio.7b01039.
[31] Kurnik M, Sahin C, Andersen CB, Lorenzen N, Giehm L, Mohammad-Beigi H, Otzen DE. Potent α-synuclein aggregation inhibitors, identified by high-

throughput screening, mainly target the monomeric state. Cell Chemical Biology 2018;25(11):1389–402. https://doi.org/10.1016/j.chembiol.2018.08.005. e9.
[32] Markowicz-Piasecka M, Huttunen KM, Sikora J. Metformin and its sulphonamide derivative simultaneously potentiateanti-cholinesterase activity of donepezil and inhibit beta-amyloid aggregation. Journal of Enzyme Inhibition and Medicinal Chemistry 2018;33(1):1309–22. https://doi.org/10.1080/14756366.2018.1499627.
[33] Podder A, Pandit M, Narayanan L. Drug target prioritization for alzheimer's disease using protein interaction network analysis. OMICS 2018;22(10):665–77. https://doi.org/10.1089/omi.2018.0131.
[34] Pujols J, Peña-Díaz S, Lázaro DF, Peccati F, Pinheiro F, González D, Ventura S. Small molecule inhibits α-synuclein aggregation, disrupts amyloid fibrils, and prevents degeneration of dopaminergic neurons. Proceedings of the National Academy of Sciences 2018;115(41):10481–6. https://doi.org/10.1073/pnas.1804198115.
[35] Ramesh M, Makam P, Voshavar C, Khare H, Rajasekhar K, Ramakumar S, Govindaraju T. l-Dopa and dopamine conjugated naphthalenediimides modulate amyloid β toxicity. Organic and Biomolecular Chemistry 2018;16(41):7682–92. https://doi.org/10.1039/c8ob01691g.
[36] Sanjeev A, Mattaparthi VSK. Computational study on the role of γ-synuclein in inhibiting the α-synuclein aggregation. Central Nervous System Agents in Medicinal Chemistry 2018;18. https://doi.org/10.2174/1871524918666181012160439.
[37] Sarnataro D. Attempt to untangle the prion-like misfolding mechanism for neurodegenerative diseases. International Journal of Molecular Sciences 2018;19(10):3081. https://doi.org/10.3390/ijms19103081.
[38] Seidler PM, Boyer DR, Rodriguez JA, Sawaya MR, Cascio D, Murray K, Eisenberg DS. Structure-based inhibitors of tau aggregation. Nature Chemistry 2017;10(2):170–6. https://doi.org/10.1038/nchem.2889.
[39] Skolnick J, Gao M, Roy A, Srinivasan B, Zhou H. Implications of the small number of distinct ligand binding pockets in proteins for drug discovery, evolution and biochemical function. Bioorganic & Medicinal Chemistry Letters 2015;25(6):1163–70. https://doi.org/10.1016/j.bmcl.2015.01.059.
[40] Zhou H, Gao M, Skolnick J. Comprehensive prediction of drug-protein interactions and side effects for the human proteome. Scientific Reports 2015;5(1). https://doi.org/10.1038/srep11090.